Online Monitoring of the Particle Size in Semibatch Emulsion Copolymerization Using Spatially Resolved Spectroscopy and Raman Spectroscopy

Manis Gheghiani, Noémie Caillol, Timothy Mckenna, Nida Sheibat-Othman

Online monitoring of the particle size in semi-batch emulsion co-polymerization using spatially resolved spectroscopy and Raman spectroscopy

Manis Gheghiani[1], Noémie Caillol[2], Timothy McKenna[3], Nida Sheibat-Othman[1*]

[1] *University of Lyon, University Claude Bernard Lyon 1, CNRS, LAGEPP UMR 5007, F-69100, Villeurbanne, France*

[2] *Axel'One, Solaize, France*

[3] *University of Lyon, University Claude Bernard Lyon 1, CPE Lyon, CNRS, UMR 5265, C2P2-LCPP group, Villeurbanne, France*

**Corresponding author:* *nida.othman@univ-lyon1.fr*

Abstract

Spatially resolved spectroscopy (SRS), based on near infrared, is better adapted to extract physical information (here the particle size) than classical spectroscopy in a heterogeneous media (suspension, emulsion, powder, foam…). It was employed to monitor the particle size in emulsion copolymerization. The prediction of the particles size was distinguishable from the prediction of the polymer content, based on their different impact on the spectra due to scattering and absorption phenomena. Models based on the partial least square regression were developed. Different types of mean diameters were studied to explore the sensitivity of the SRS and the possibility to reconstruct the particle size distribution. Raman spectroscopy was also investigated to determine the impact of particle size on the signal and how far it can be quantitative.

Keywords: Spatially resolved spectroscopy, Raman spectroscopy, emulsion polymerization, scattering, particle size distribution

1. Introduction

In heterogeneous polymerization processes, such as emulsion and suspension polymerizations, the reaction takes place in the dispersed phase. A wide variety of polymers with different properties can be produced by these processes, such as adhesives, rubbers and plastics. However, the heterogeneous nature of these processes makes them more challenging to monitor and control than single phase processes.

Monitoring the progress of the reaction, such as the monomer conversion or the reaction rate, constitutes a first step towards a good control of the process.[1] Concerning the quality of the product, it may be affected by both chemical and physical properties that are important to monitor. At the molecular scale, monitoring the polymer molecular weight is essential as it affects the polymer mechanical properties and viscosity.[2,3] Also, several processes involve more than one monomer in order to modulate the product properties by changing the chemical composition [4] that plays a significant role in the end-use properties such as the polymer glass transition temperature and adhesion. For instance, the polymer composition was monitored by spectroscopy.[5–7]

In heterogeneous polymerizations, additional challenges are present as the polymerization does take place in the particles dispersed in a continuous phase. It is therefore important to monitor the particle size distribution (PSD) as it affects the polymer quality (e.g. film quality, visual aspect) as well as the progression of the reaction (e.g. mass and heat transfer, viscosity, stability). The particle size can be measured by different offline techniques, such as optical or electron microscopy[8], dynamic light scattering (DLS) mainly for nanometer scale particles[9], or laser diffraction for micrometer and nanometer scale particles.[10] These techniques require however sampling and dilution.

Based on the light-matter interaction, spectroscopy is expected to contain information about the particle size besides the chemical composition. Frequently, to extract only the chemical information, the *physical* information is removed from the spectral data using different pre-processing methods, such as multiplicative scatter correction or standard normal variate transformation.[11,12] This makes it possible to apply Beer-Lambert law to quantify the chemical composition. More recently, some studies have employed spectroscopy to predict the particle size. In the case of Raman spectroscopy, studies have been done offline in order to find a quantitative or qualitative correlation with the particle size for styrene, butadiene, methyl methacrylate and acrylonitrile latexes [13]. Few online studies have also been done for styrene/acrylic acid[14] or styrene/butyl acrylate emulsion co-polymerizations.[15] A good agreement was shown but for a limited range of particle size, going from 50 to a maximum of 150 nm.

Some studies have also employed near infrared spectroscopy (NIR) to predict the particle size, for instance in the emulsion polymerization of methyl methacrylate[16], copolymerization of styrene/butyl acrylate[17,18] or copolymerization of vinyl acetate/butyl acrylate[19], butyl acrylate/styrene miniemulsion copolymerization[20], dispersion polymerization[21], styrene suspension polymerization[22] and vinyl chloride suspension polymerization[23], where the particle size varies between tens of nanometers to few millimeters between these systems. These studies demonstrated that the NIR spectrum is affected by the particle size distribution. In these works, the spectrum was treated to remove other chemical effects and only focus on the particle size. The ability to predict the particle size with infrared spectroscopy can be explained by different phenomena due to the light-matter interactions that affect the collected data. First of all, the chemical species present in the particles may absorb part of the energy (i.e. photons) of the incident light. This affects both the transmitted and reflected

energies. The magnitude of absorption of light at different wavelengths is a function of the nature of the species and thus contains information about the chemical composition. A second phenomenon appears mainly in heterogeneous systems that cause light deflection, and is called the scattering phenomenon. Different cases of scattering can be observed according to the properties of the particles (size and shape among others). For a spherical particle of size smaller than the excitation wavelength (λ), Rayleigh theory (which is an approximation of Mie theory) indicates that the scattering cross section (i.e. the probability of a particle to scatter the light) is dependent on $1/\lambda^4$.[24,25]

When the absorption and scattering phenomena of light by particles are significant, only a fraction of the incident light is transmitted and so transmission spectroscopy only contains a part of the information of the medium. Therefore, different technical solutions have been proposed to collect both transmission and scattering information, like the integrating sphere [26] or temporal resolved spectroscopy[27] which can be used for offline or static measurements. Another solution, that is considered in this work, is the spatially resolved spectroscopy (SRS) which is based on NIR spectroscopy and can be used online and *in situ*.[28,29] For instance Chen et al. 2017 used a spatial resolved diffuse reflectance measurement system with light sources at different incident angles (0°, 30°, 45°) to improve the signal content of the measured spectra and estimate the particle size of polystyrene particles, in the range of 50 to 250 nm[30]. In this technology, the light is collected at different angles from the incident light, enabling to collect both the transmission and scattering information. Note that in conventional *in situ* NIR spectroscopy probes, data is collected only at one angle, either by transmission at 180° or by reflection at usually less than 30°. The SRS used here also collects data in the transmission direction at 180°, but also in the scattering directions at 175° and 170°, and one angle in the backscattering direction at 30°. It is therefore supposed able to give more information about

the physical state of the complex heterogeneous medium (e.g. particle size). This technology therefore assures relevant characterization at least at one angle whatever the evolution of the complex medium, from transparent to opaque, during the process. The aim of this work is to evaluate the potential of the SRS to determine the particle size in emulsion copolymerization. Different ways of calculating the mean diameters from the distribution are investigated to identify to which one the SRS is more sensitive and eventually reconstruct the particle size distribution (PSD) from these diameters.

The paper is organized as follows: In the first part, the potential of SRS spectroscopy is investigated. An offline study is first done to investigate the impact of the particle diameter and concentration on the spectra. Then, polymerization experiments are designed to ensure decoupling between the particle size and the polymer content. A predictive model based on Partial Least Squares is developed using a selection of training samples. Different types of mean diameters are considered. Then, a predictive model is evaluated using external data to evaluate the limits and the potential of the model and the technology. The reconstruction of the full particle size distribution is also considered. In the second part, Raman spectroscopy is considered, starting with a similar offline study. Then, an online study, using the same experiments as for SRS, is done with the development of regression models based on Partial Least Squares.

2. Materials and method

2.1 Materials

The monomers used in this study are methyl methacrylate (MMA, Acros Organics, 99%, stabilized) and butyl acrylate (BuA, Acros Organics, 99+%, stabilized). The initiator is potassium

persulfate (KPS, Acros Organics, 99+%). The monomers and initiator were stored in a fridge until used. Sodium dodecyl sulfate (SDS, Fisher Chemical) was used as ionic surfactant. Deionized water with an 18 MΩ cm resistivity was used throughout the work.

2.2 *Seeded* semi-continuous polymerization experiments

A 1 L reactor was used with mechanical stirring at 300 rpm using a three blade Bohlender propeller. The standard protocol of seeded experiments consisted in using a diluted latex, previously produced in *ab initio* or seeded experiments under similar conditions, for which the particle size, SDS content and solids content are known. The diluted latex was degassed using nitrogen for 30 min under stirring and heated to 70 °C using a thermostated bath. 200 g of a MMA/BuA mixture, with 70 % wt of MMA and 30 % wt of BA, was then placed on a balance and semi-continuous monomer addition was started at a flow rate of 0.02 g/s. Simultaneously, 1.6 g of KPS was dissolved in the reaction medium to initiate the reaction. At the beginning of the reaction, the nitrogen gas flow was moved to the top of the reactor, to maintain saturation of the gaseous atmosphere with nitrogen. Temperature measurements in the reactor and the jacket were measured and a controller allowed maintaining the reactor temperature at 70°C. Also, the mass of monomer on the balance was measured to ensure a constant monomer flow rate at 0.02 g/s by an automatic control of the pump. Samples were collected at specific time intervals to measure the solids content (*i.e.* mass fraction of solid) using a thermobalance (Mettler Toledo LJ16); with the mass of surfactant and initiator subtracted from the solids content to calculate the mass fraction of polymer. The particle size distribution was measured using dynamic light scattering (DLS, Malvern Nano ZS®).

2.3 Design of experiments

Experiments were realized in a way to vary the particle size of the latex over a wide range of industrial interest, and at the same time to ensure decorrelation of the variations in the size from the solids content. Indeed, in emulsion polymerization, an increase in the solids content during the reaction usually implies an increase in the particle size, especially if nucleation and coagulation of particles are negligible. Therefore, carrying out only *ab initio* experiments (as though frequently done in the literature) may not have allowed proper decoupling between these variables which may lead to big errors when developing predictive models based on multivariate spectroscopic models. By carrying out seeded experiments, it is possible to start the reaction with various solids content and various particles sizes. Such a choice of experiments should allow the model to predict the particle size independently of the solids content and progress of the reaction.

The realized experiments are shown in Table 1, indicating the solids content and the mean particle diameter provided by the DLS (z-average). Note that in experiments 1-4, the particle size was varied from 48 to 550 nm with complete decoupling from the initial solids content which was varied from 2.2 to 25 % by weight. To add further variability, experiments 2, 9 and 10 were designed to have the same initial size (117 nm) but different initial solids content (about 4.5 and 8.5 % wt), with experiment 2 being the most diluted and experiment 10 the most concentrated. Finally, in experiments 11 and 12 a perturbation was caused on purpose at the middle of the reaction in order to simulate a renucleation. To do so, after 100 minutes of the reaction in experiment 11, the latex was partially emptied from the reactor (at this stage the particle size was about 280 nm and the solids content 20 % wt). Then, 400 g of the latex from experiment 5 with smaller particles was added to the reactor (142 nm, at 22.8 % wt,

heated to 70°C). As a result, the reactor contained approximately a 50-50 % mixture of latex with sizes 280 nm and 142 nm (with similar temperature and solids content). In experiment 12, almost the same modification in size was done (a 142 nm latex is added to a 250 nm latex) but with a ratio of the number of small particles to big particles of about 45:55 %.

Table 1: Solids content range and z-average range for the different experiments realized

Experiment	*Solids content range (% wt)*	*Particle diameter range (z-average, nm)*
1	2.2 - 13.6	48 - 73
2	4.3 - 22	117 - 195
3	4.4 - 23.4	195 - 345
4	9.7 - 23.9	345 - 550
5	5.6 - 22.8	73 - 142
6	6.6 - 25.4	195 - 372
7	5.5 - 23.6	195 - 338
8	7 - 26.2	195 - 381
9	4.6 - 20.8	117 - 210
10	8.5 - 20.4	117 - 167
11	3.8 - 16.4	210 - 280
12	5.5 - 17.2	167 - 246

2.4 SRS spectroscopy

A multiangle probe Sam-Flex (Indatech®, Chauvin Arnoux) was connected to a spectrometer from Indatech® (Hyternity) which is composed of a NIR InGaAs camera. The measurement is done simultaneously with a 3 mm pathlength at four angles which are positioned as follows: one angle in the transmission direction at 180° (according to the light source), two angles in the scattering directions at 175° and 170°, and one angle in the backscattering direction at 30° [31]. From this configuration, the 175° angle can be thought to be more sensitive to simple scattering, while the angle at 170° is more sensitive to the multiple scattering and the angle at 30° is more sensitive to backscattering. The NIR spectral domain was from 871 nm to

1723 nm for each angle, with a 3 nm interval. For all the acquisitions, the integration time was 70 ms with 100 scans, for a total acquisition time of 7 s. The acquisition was made every 15 s. The acquisition time was fixed in a way to maximize the intensity while avoiding saturation of the detector. As different intensity levels are measured at the four angles, attenuators are available to tune the intensity of light measured at each angle. Physical attenuators were thus set on manually at 180° and 175° in order to avoid saturation of the signal at the beginning of the reaction where the medium is diluted and the transmission signal is very strong.

2.5 Dynamic light scattering (DLS)

A Malvern Nano ZS® was used to measure the particle size offline. This technology relies on photon correlation spectroscopy (PCS). The samples taken from the reactor were put in an ice bath to stop the reaction. They were then diluted with deionized water of 18 MΩ cm resistivity to reach an attenuation coefficient between 4 and 5. The mean diameter given by this device is the z-average, which is the intensity-based harmonic mean (2,3) calculated from the scattering intensity weighted distribution. The z-average and the particle size distribution (PSD) in volume and number were collected. The number-weighted PSD was then used to calculate various types of particle mean diameters which will be discussed later on.

2.6 Chemometrics

A data pre-processing approach was employed [31], including data smoothing using a Savitzky-Golay filter [32] with 15 points averaged with a polynomial of second order, followed by a first order derivative. A prediction model of the particle size was then developed based on Partial Least Square (PLS) regression using the Nonlinear Iterative Partial Least Square (NIPALS) algorithm [33]. In the case of Raman, an offset correction of the baseline was first applied by

subtracting the intensity at 2000 cm^{-1}, where no band is present, to the whole spectrum. All the chemometric study was carried out using Matlab®.

3. Results and discussions

3.1 Types of mean diameters

The DLS, here Nano ZS, provides an intensity weighted measurement of the PSD, based on Rayleigh scattering which is proportional to d^6. From this distribution, the distributions in number and in volume are calculated, based on the Mie's theory. It is then convenient to calculate a mean diameter in order to characterize the latex. In the present work, it is also important to define the type of mean diameter to which the SRS spectra are most sensitive. Several types of mean diameters can be calculated from the PSD in number (f_i) by using equation 1:

$$d_{m,n} = \frac{\sum f_i d_i^m}{\sum f_i d_i^n} \quad (1)$$

The volume-weighted mean diameter, d_{43}, also called the De Brouckère mean, is the ratio of the 4th moment to the 3rd, while the surface-weighted mean diameter d_{32}, also called the Sauter mean diameter, is the ratio of the 3rd moment to the 2nd. The number mean diameter d_{10} is also of interest mainly in order to reconstruct the PSD. The PSD in volume is proportional to the volume of particles, so $f_{\mathrm{vol}\_i} = f_i \pi d_i^3/6$ as the particles are considered to be spherical. Bigger particles have a higher impact in the volume distribution (and even higher in the intensity distribution). Generally, the median dv_{50} is used to describe the volume distribution, which corresponds to the diameter where half of the polymer volume has smaller particle size and the other half is larger. The dv_{10} and dv_{90}, correspond respectively to diameters where 10

% and 90 % in volume of the particles have a smaller diameter. The Nano ZS calculates the Z-average mean diameter (intensity-based harmonic mean) as a hydrodynamic diameter, d_H, using the Stokes-Einstein equation:

$$d_{\mathrm{H}} = \frac{kT}{3\pi\eta D} \quad (2)$$

with T the temperature, k the Boltzmann's constant and η the dynamic viscosity of the continuous medium. The translational diffusion coefficient D is calculated from an auto-correlation function based on the variations of intensity during the measurement.[34]

In the case of monomodal and narrow distributions (see Figure 1a, z-average 73 nm), the different types of diameters are almost equivalent in terms of their evolution and the importance given to a specific size. However, multimodal or wide distributions (see Figure 1b, z-average 435 nm) generate bigger differences between the PSD in number, volume and intensity. Therefore, the difference between the different mean diameters increases because of the wider distribution and one needs to decide which one is more descriptive of the sample for a specific application. Note that the distribution can broaden during the reaction because the particles do not grow at the same rate and they do not undergo similar coagulation rates, due to different probabilistic or mixing issues.

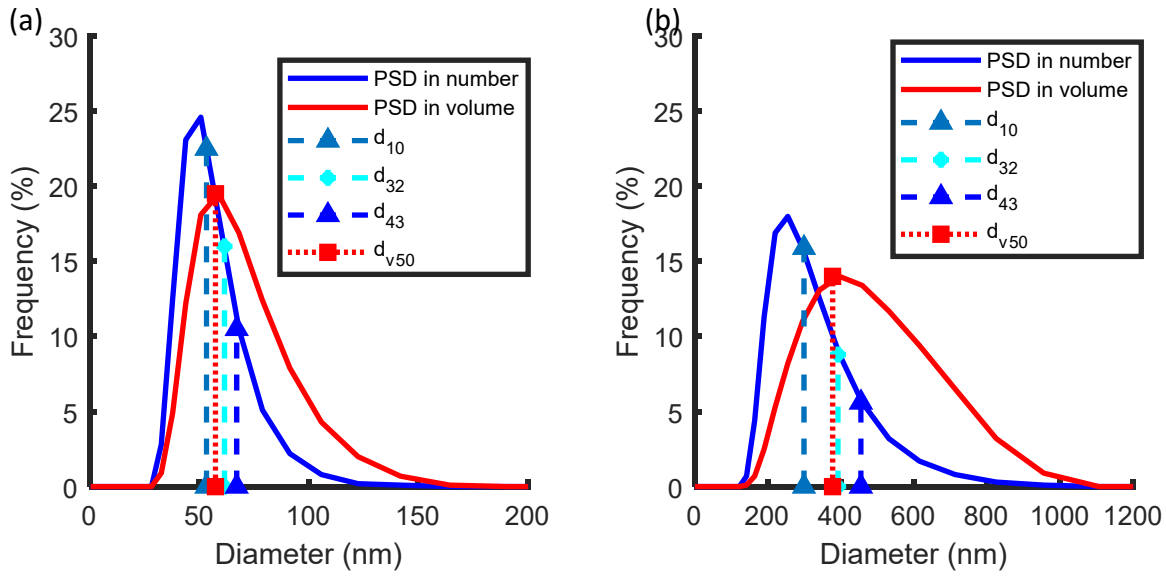

Figure 1: Particle size distribution in number and volume indicating the mean diameters d_{10}, d_{32}, d_{43} and dv_{50} a), Z-average = 73 nm, b) Z-average = 435 nm

3.2 Offline investigations of the SRS

Latex samples were prepared with different particle size and solids content and the SRS spectra were collected for each one. The objective was to study the impact of the particles diameter at a known concentration on the spectra. Mixtures of latexes of different sizes were also prepared to study the effect of the size bimodality on the SRS measurement. Samples were heated at 70°C to be representative of the process conditions, as the temperature is known to impact the spectra in the NIR region.

Figure 2a shows the SRS spectra of samples with the same solids content (16 % wt) but with different particle sizes, with a z-average varying from 70 nm to 550 nm. As a reminder, the angles at 180°, 175°, 170° and 30° from the light source correspond respectively to the transmission, simple scattering, multiple scattering and backscattering phenomena. It can be seen that the intensity of the spectra collected at 180°, 175° and 170° decreases when the particle size increases, with the intensity at 180° decreasing the fastest and at 170° the slowest. It can be deduced that the increase in the particle size first reduces the transmission

and simple scattering to almost no signal when the z-average is equal or bigger than 195 nm (at a concentration of 16 % wt). The multiple scattering signal (170°) also decreased, but it was still non null when the particle size was 195 nm, and then decreased significantly for particles of 345 nm. Concerning the signal at 30°, it had an opposite behavior as the intensity increased with the particle size. Indeed, big particles are more likely to reflect the light thus causing more backscattering. The difference in intensity between the spectrum for particles of 345 nm and 550 nm is smaller than between 195 nm and 345 nm. Indeed, the scattering phenomenon is nonlinear [35] and depends on the difference between the size of the particle and the wavelength of the light. Also, in the experiment with 550 nm, the latex started to be non-uniform as some coagulum appeared, and therefore the offline measurement by DLS might not be representative. In conclusion, the offline study validates the fact that the SRS contains information about the particle size, independently of the latex concentration, that can be used for monitoring.

Figure 2b shows the evolution of the spectra when changing the solids content at a constant particle size (z-average of 195 nm). As the particle size is constant, an increase in the solids content is equivalent to an increase in the number of particles per unit volume. It can be seen that the signals at 180°, 175° and 170° decrease with the increase of the solids content while the signal at 30° increases, as in the study of the particle size effect. However, the magnitude of the variations is different from the one observed with the particle size, which should allow distinguishing between them by calibration. The impact of concentration on the spectra is not investigated further here as monitoring of the solids content by SRS has already been studied in a previous work and its feasibility was demonstrated [31].

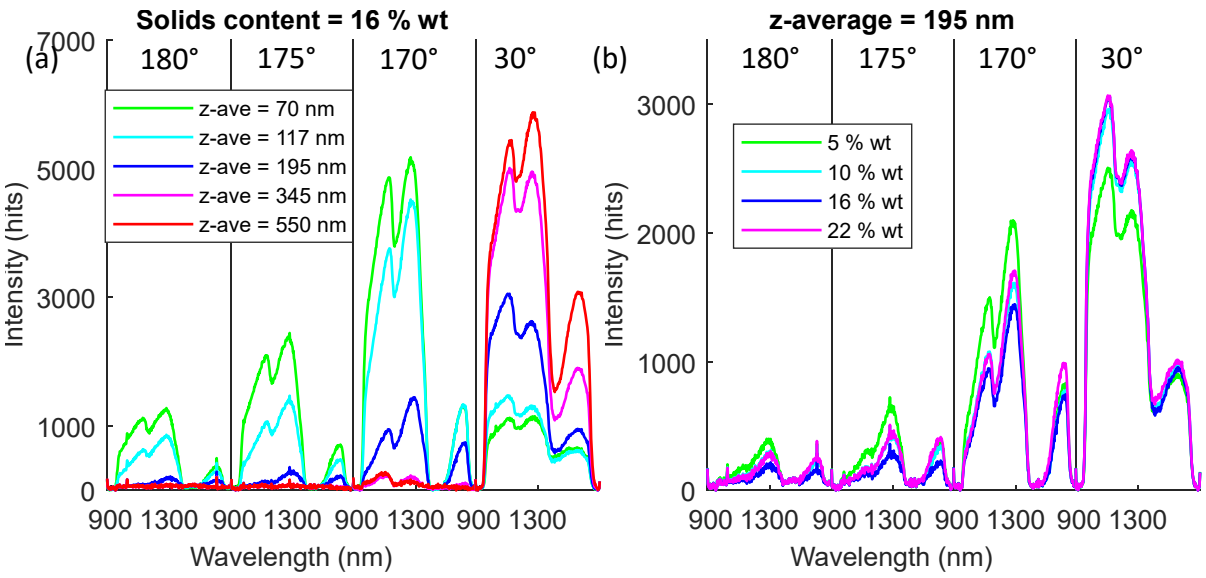

Figure 2: SRS spectra of samples with (a) 16 % wt of solids content and different particles sizes, (b) 195 nm and different solids contents

Mixtures of latexes of different sizes, with a mass ratio of 1:1 at 16 % wt, were prepared to study the impact of size bimodality on the SRS data. Figure 3a shows the SRS spectra of latexes with z-average of 70 nm, 550 nm and their 1:1 mixture. It can be seen that for particles of 70 nm, the signal is non-null at all angles while for particles of 550 nm it is mainly present at 30° (with almost 6000 hits), a little at 170° (less than 200 hits) and null for the others angles, as big particles stop transmission as well as simple scattering at the studied concentration. As a result, the SRS spectra corresponding to the mixture show no signal at 180° and 175°, a small signal at 170° relatively close to the spectrum of 550 nm, and a maximum of intensity around 4 000 hits at the angle 30°. For this angle, the signal is in between the spectra of the unimodal latexes of sizes 70 and 550 nm. The observed phenomena in the mixture seem to be dominated by the biggest particles, because only the backscattering angle, 30°, shows a signal and not the others.

Figure 3b shows the SRS spectra with a z-average of 70 nm, 195 nm and their 1:1 mixture. It can be seen that the signal is present at every angle for each for the three products, as no big particle sizes are present. The spectra of the mixture are in between the unimodal spectra as observed previously. However, in this case all the phenomena (transmission, simple, multiple and backscattering scattering) are present (i.e. the intensity signal is non-null for all angles). The gap in the z-average is not as big as previously so the biggest particles do not totally govern the light-matter interaction. These observations indicate that the SRS can be sensitive to a second population of particles that can be detected. This can be useful in emulsion polymerization for instance to detect renucleation or sudden particle coagulation if the gap between them is not too important.

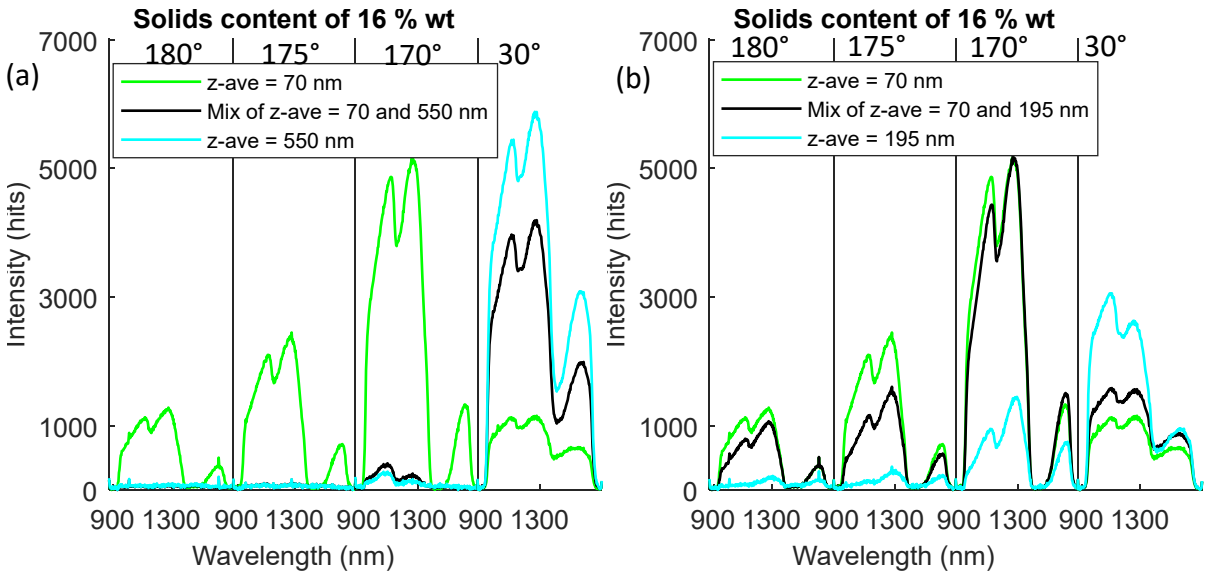

Figure 3: SRS spectra at different angles for monomodal latexes of different sizes and their mixtures (at 16% solids content): (a) 70 and 550 nm, (b) 70 and 195 nm.

3.3 Online implementation of the SRS

3.3.1 Building and comparison of the models for different types of diameters

As the angles 180°, 175° and 170° have no signal for almost half of the range of the studied particle size, they will not be included in the PLS prediction model. Only the 30° signal will be used as it contains the biggest amount of information in the present application. The potential of the SRS is thus not fully exploited in this study as only one angle is used for building the models. However, the other angles can be useful for other ranges of sizes or concentrations or by changing the attenuator to avoid saturation and absence of the signal in the whole range. The calibration models were built using part of the online experiments, for which a higher amount of data is available for training and validation. Experiments 3, 6 and 8 were used for external validation. The data from experiment 4 (z-average of 550 nm) were not included in the development of the calibration model due to the presence of some bubble in the probe and coagulation phenomenon. The other experiments were used as follows: 2/3rd to build the calibration model and 1/3rd for validation. To do so, the experiments were organized from the one generating the smallest particles to the one generating the biggest particles, then 2 samples out of every 3 were selected for calibration. A total of 66 samples were used, with 44 for the development of the calibration model and the 22 remaining for internal model validation.

Figure 4 shows the z-average for the experiments used to build the calibration model (runs 1, 2, 5, 7, 9 to 12) as a function of the solids content. It can be seen that the data are within the same range of solids content, from 2 to 25 % wt, while multiple z-average are available for one solids content (ranging from 48 nm to 350 nm). This is essential in order to ensure decoupling between these two variables.

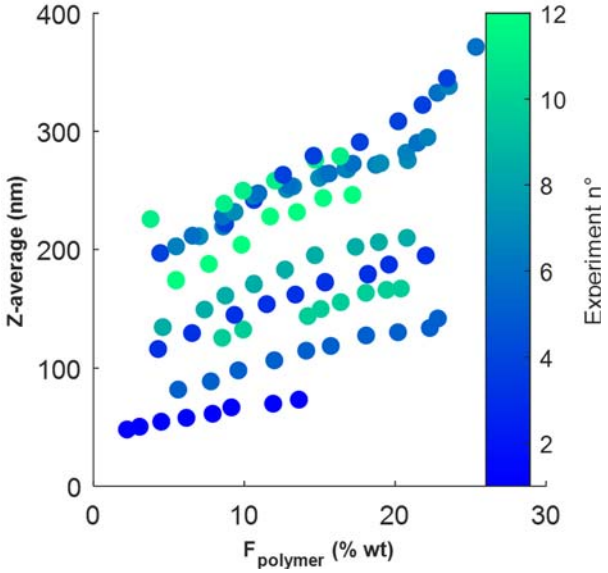

Figure 4: Z-average according to the solids content of the experiments used for model development

To ensure the best model sensitivity, calibration models were developed for different type of mean diameters: z-average, d_{10}, d_{32}, d_{43} and dv_{50}. The choice of the number of latent values (LVs) was made by using cross-validation with a leave-one out cross-validation and 3 repetitions with a Monte-Carlo cross-validation algorithm. The general rule is to take the minimum number of LV sufficient enough to describe the desired phenomenon. Selecting more LVs is known to lead to overfitting. Figure 5a shows the root mean square error of cross-validation (RMSECV) with a plateau for 5 LVs and a minimum for 10 LVs. The reasonable choice here is 5 LVs, to avoid overfitting and increasing sensitivity to noise. Similar observations were obtained for the other models developed on this dataset. Therefore, 5LVs were always chosen.

Figure 5b shows the parity diagram of PLS regression obtained with 5 LVs. The obtained root mean square error of calibration (RMSEC) and prediction (RMSEP) are respectively 8 nm and 7 nm. The standard deviation of the DLS (the reference method) is 5 nm. The RMSEC and

RMSEP are close to the DLS value so the uncertainty of the model is acceptable. A confidence interval of 95 % was chosen, so twice the standard deviation of the DLS, which makes 10 nm. It can be seen on the parity diagram that the majority of the data are within this interval.

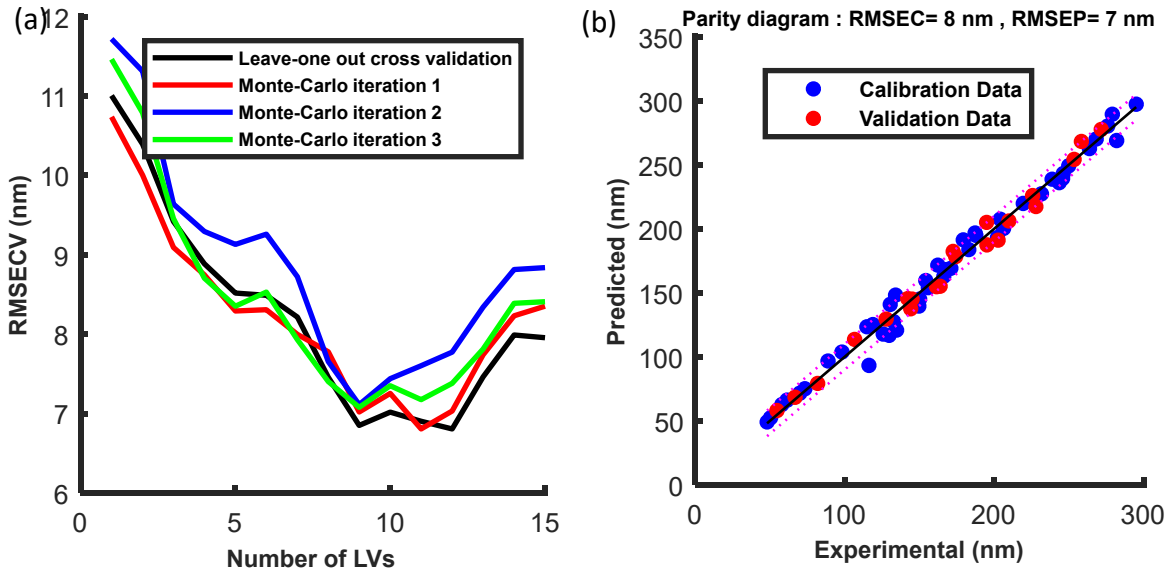

Figure 5: (a) Root mean square error of cross-validation according to the number of latent values using leave-one out (black) and 3 iterations of Monte-Carlo algorithm (red, blue, green) and (b) Parity diagram of the data points predicted using partial least square (PLS) regression to predict the z-average with 5 LVs

The same methodology was applied to develop models to predict d_{10}, d_{32}, d_{43} and dv_{50}. Table 2 recaps the RMSEC and the RMSEP for these models, with 5 LVs. It can be seen that the RMSEC are quite similar for all models. However, the RMSEP shows some differences, with values of 7, 6, 9, 15 and 10 nm respectively for the models of z-average, d_{10}, d_{32}, d_{43} and dv_{50}. A much higher RMSEP is obtained for d_{43} compared to the other diameters. As a reminder, only the angle 30° is used, and the use of the other angles of SRS may improve the prediction of d_{43}, which is volume-based.

Table 2: Root mean square error of calibration (RMSEC) and prediction (RMSEP) obtained from the models based on z-average, d_{10}, d_{32}, d_{43} and dv_{50}

Diameter	*RMSEC (nm)*	*RMSEP (nm)*
Z-average	8	7
d_{10}	9	6
d_{32}	9	9
d_{43}	9	15
dv_{50}	8	10

In order to evaluate the sensitivity of the five models, the beta coefficients of the PLS regression are compared (Figure 6). It can be seen that the contribution of the different wavelengths for z-average and d_{32} are quite similar in shape all over the spectrum but they differ in the absolute value of the coefficient. The same observation can be made between d_{43} and dv_{50}, which have the same trend but the coefficients of d_{43} have much higher absolute values all over the spectral range. The d_{10} coefficients are not similar as the other diameters. The different mean diameters do not evolve at the same rate when the particle size increases and this can explain why different coefficients are obtained. These observations show that different ways of calculating the mean diameters lead to different models and the diameter, that is correlated to clear changes in the spectra, needs to be chosen carefully.

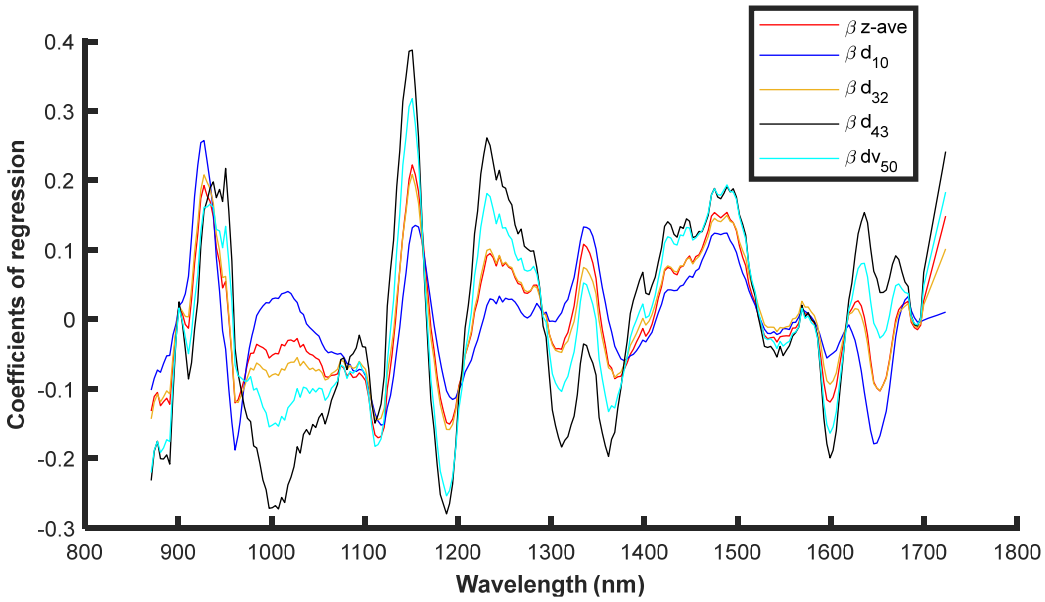

Figure 6: Beta coefficients of the PLS regression models based on different types of mean diameters

Figure 7a compares the predictions of the different mean diameters in experiment 2, partly used to build the calibration model. All the predictions follow the trend of the reference measurements correctly. An overestimation of the particle diameter by the SRS compared to the DLS can be observed for the d_{43}, as was noticed by its high RMSEP in Table 2. Figure 7b shows the prediction of z-average for the experiments 1, 2, 5 and 7, also partly used in the calibration data. It can be seen that the prediction fits well with the DLS measurement all over the particle diameter range.

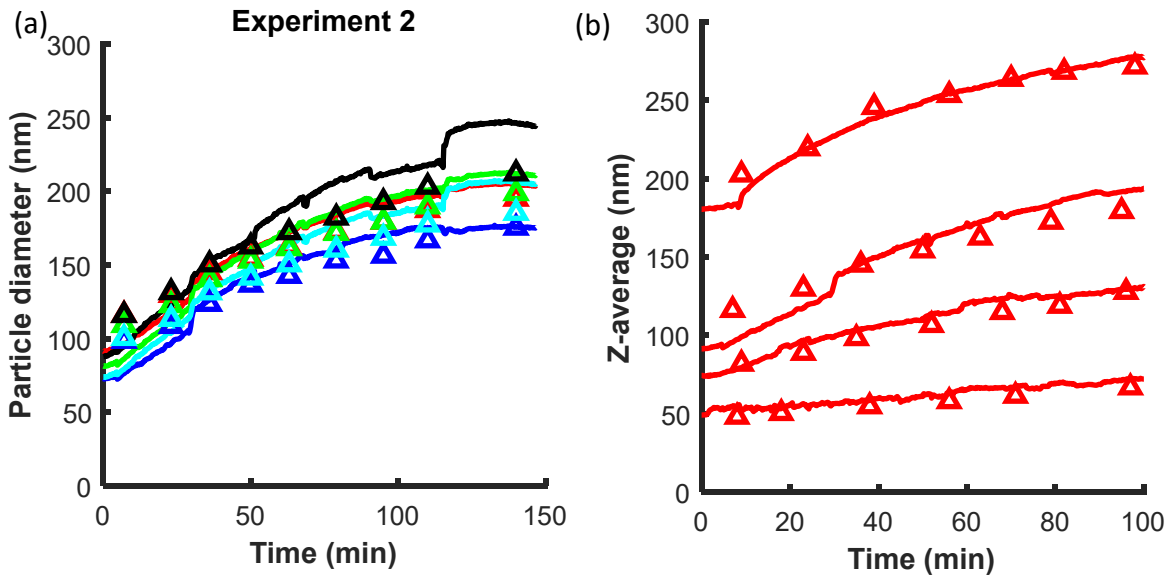

Figure 7: (a) Prediction of z-average (red), d_{10} (dark blue), d_{32} (green), d_{43} (black) and dv_{50} (cyan) for experiment 2 by the SRS model of prediction; and (b) Prediction of z-average for experiments 1, 2, 5 and 7 (from bottom to top) according to time. The predictions are given by the continuous line and the experimental values by the symbols.

An external validation has been done with the runs not used to build the calibration model. Figure 8 shows the predictions of all types of diameters for experiment 8. Some differences between the DLS values and SRS predictions are observed, but in general the estimations remain acceptable.

It can be concluded that the SRS data gives similar predictions of all the diameters, except the d_{43} which is less accurate. The other types of mean diameters are almost equivalent in terms of RMSEC and internal and external validation, and they all can be implemented.

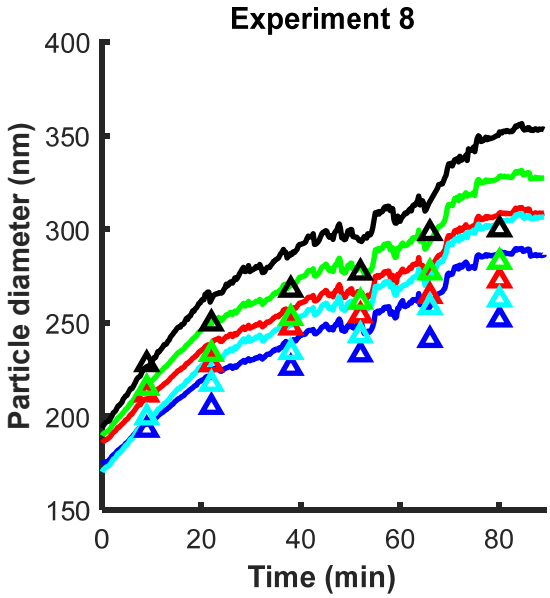

Figure 8: Prediction of z-average (red), d_{10} (dark blue), d_{32} (green), d_{43} (black) and dv_{50} (cyan) for experiment 8 with the SRS models of prediction. The predictions are given by the continuous line and the experimental values by the symbols.

3.3.2 Online investigations of the size bimodality

The offline study indicated that the SRS is sensitive to the presence of two populations of particles of different sizes. In this section, the developed model is evaluated in the case where smaller particles are suddenly introduced in the latex (that can be representative of renucleation for example). The model using the z-average is used for the discussion in this section, knowing that the other diameters (d_{10}, d_{32}, d_{v50}) give similar trends. Figure 9 shows the prediction of the z-average for experiments 11 and 12. As a reminder, at about 100 minutes a latex with smaller particles was added leading to a 50-50 % mixture latex with sizes 280 nm and 142 nm. It can be seen that the model instantaneously detects a change in the medium, and the predictions move towards smaller particles, as smaller particles are added. No comparison with the DLS is shown after this modification, as it is incorrect to characterize a bimodal latex by one mean diameter. However, it can be seen that the SRS predictions (starting at about 270 nm) are in between the sizes of the two populations present in the

reactor (280 and 142 nm), but much closer to the bigger particles. In experiment 12, a latex of 142 nm is added to a latex of 250 nm, at a ratio of small to big particles of about 45:55, and similar conclusions can be made. Therefore, it can be expected that the SRS can detect particle renucleation or coagulation during the reaction. However, in these experiments half of the mixture was replaced by smaller particles, while if renucleation or coagulation occur at a low rate, they may not have a significant impact on the SRS. Also, the offline study regarding size bimodality has shown that the phenomena caused by small particles can be hidden by the bigger ones when the difference in size is important. So, the number of particles created from renucleation or coagulation and the difference between the sizes of the two populations determine the possibility of detection by the SRS. In a comparable way, Nogueira Ambrogi et al. 2017 estimated smaller particle sizes than original droplets in miniemulsion polymerization by NIR spectroscopy, which was attributed to renucleation[20].

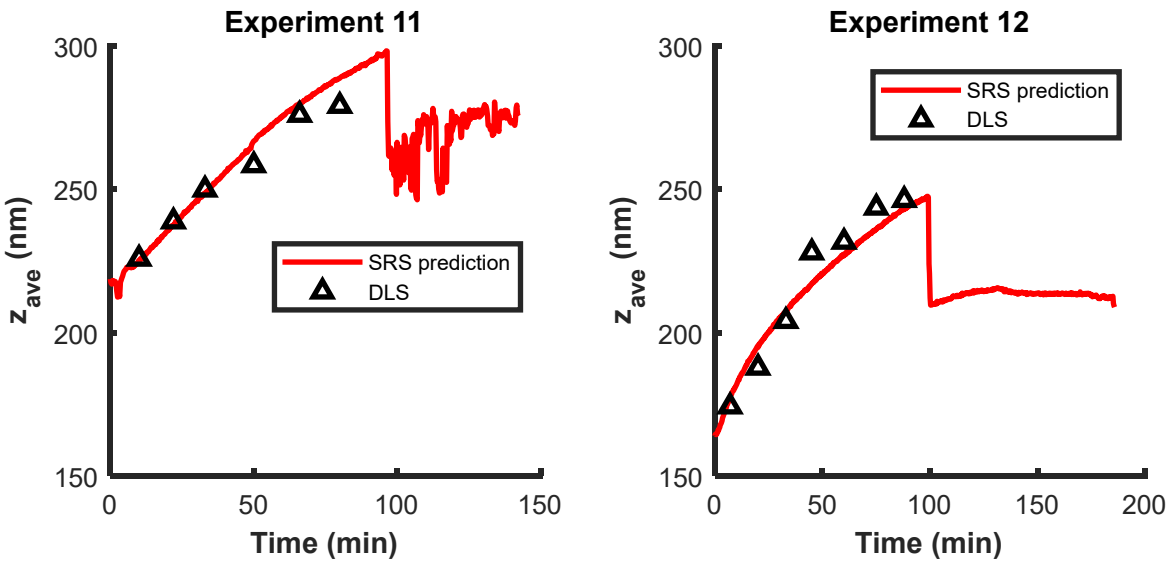

Figure 9: Prediction of the z-average in experiments 11 and 12 with addition of a latex with smaller particles size (142 nm) than the latex present into the reactor

3.3.3 Reconstruction of the particle size distribution

In this section we investigate the possibility of reconstructing the particle size distribution from the predictions of the mean diameters. In the absence of continual nucleation or occasional coagulation, the PSD can be characterized by a log-normal distribution which can be expressed as a function of the standard deviation, σ_x, and, the mean of the distribution, d_{10}, (where *x* is the vector of sizes):

$$f(x) = \frac{1}{x\sigma\sqrt{2\pi}} e^{\left(-\frac{(\ln x-\mu)^2}{2\sigma^2}\right)}, \text{ with } \mu = \ln\left(\frac{d_{10}^2}{\sqrt{d_{10}^2+\sigma_x^2}}\right) \text{ and } \sigma^2 = \ln\left(1+\frac{\sigma_x^2}{d_{10}^2}\right) \quad (3)$$

The mean diameter d_{10} is available by the SRS, but the standard deviation is unknown. As the standard deviation is not a direct physical property, even though it is related to the fraction of particles with different sizes which do have an impact on the spectra, it was not possible to make a good model of it directly from the spectra. The standard deviation and the PSD can be estimated from the other predicted diameters indirectly. In order to do so, the standard deviation is estimated using an optimization algorithm. The minimization criterion, J, is given by (equation 4):

$$\min_{\sigma_x, d_{10}} J = \left(d_{10,\text{model}} - d_{10,\text{SRS}}\right)^2 + \left(d_{32,\text{model}} - d_{32,\text{SRS}}\right)^2 + \left(d_{43,\text{model}} - d_{43,\text{SRS}}\right)^2 \quad (4)$$

Where $d_{10,\text{model}}$ $d_{32,\text{model}}$ and $d_{43,\text{model}}$ are calculated from the log-normal distribution by applying equation 1. Note that d_{10}, besides σ_x, was also optimized by this equation (while available by SRS), which was found to improve the estimations of the distributions.

Figure 10 compares the number size distributions obtained using the DLS and the reconstructed distribution based on the SRS predictions, for different latexes with z-average of 48, 142, 210 and 295 nm. It can be seen that the recalculated PSD fits really well the PSD

obtained by DLS. For small particles, the maximum of the peak is not well estimated, while for bigger particles the recalculated PSD fits perfectly the real PSD. Note that, as shown previously (Figure 1), when the particles are bigger, the distribution becomes larger and the distance between d_{10}, d_{32} and d_{43} increases, which may enhance the distinction between them. It can be concluded that the use of the diameters predicted by SRS allows to reconstruct the PSD with satisfactory results, which allows predicting the PSD online without sampling.

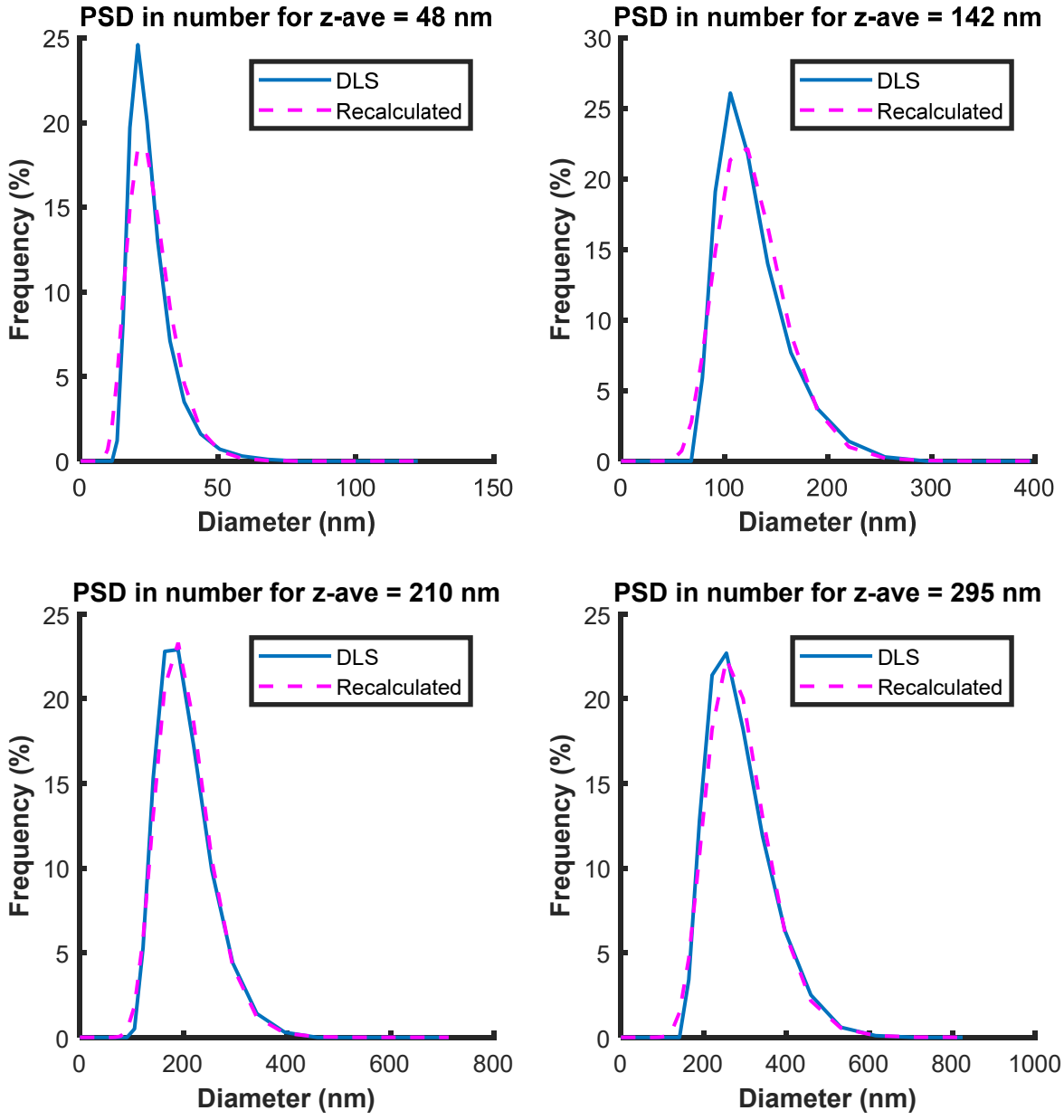

Figure 10: PSD in number obtained from DLS and recalculated from SRS predictions for different particle sizes

3.4 Comparison with Raman spectroscopy

In parallel to the SRS monitoring, Raman data were acquired first offline to study the effect of the particle size on the spectra and then online during the same experiments as SRS. The results can be found in Supporting Information.

4. Conclusion

The use of NIR spatially resolved spectroscopy and Raman were investigated for the monitoring of the particle size in emulsion copolymerization. The experiments were designed in a way to decouple variations in the particle size from the solids content. The solids content range was limited to 25 % wt to avoid fouling of the probes. PLS was used for model development. Different mean particle sizes were predicted and compared.

Offline investigations demonstrated that the SRS is sensitive to changes in the particle size, particle concentration (or solids content) and the presence of a bimodal latex. Changes in the particle size had different effects on the spectra than for the solids content. The calibration was done using part of the online data. By keeping similar solids contents for different ranges of diameter, and vice versa, we have ensured that the diameter of particle was totally decoupled from the solids content in the dataset.

Even though only the backscattering information at 30° was used, good predictions were obtained for all diameters (z-average, d_{10}, d_{43}, d_{32} and $d\mathrm{v}_{50}$) even though the d_{43} was slightly less accurate. The capacity to predict multiple diameters has allowed to recalculate the PSD in number which is a useful information to be monitored online using SRS. The study has also

shown the ability to detect bimodality offline as well as online but within particular ranges of sizes and concentrations which would need to be investigated.

On the other hand, Raman spectroscopy has demonstrated its capacity to differentiate different diameters of particles. It could give acceptable predictions of the particle size, though with a lower sensitivity than the SRS. The SRS is therefore better adapted for the monitoring of the particle size.

Acknowledgments

This work was funded by the pole Lyon Process Science and Engineering (LPSE).

Supporting information

This information is available free of charge via the Internet at http://pubs.acs.org/.

References

(1) Cherfi, A.; Févotte, G. On-Line Conversion Monitoring of the Solution Polymerization of Methyl Methacrylate Using near-Infrared Spectroscopy. *Macromolecular Chemistry and Physics* **2002**, *203* (9), 1188. https://doi.org/10.1002/1521-3935(200206)203:9<1188::AID-MACP1188>3.0.CO;2-N.

(2) Colby, R. H.; Fetters, L. J.; Graessley, W. W. The Melt Viscosity-Molecular Weight Relationship for Linear Polymers. *Macromolecules* **1987**, *20* (9), 2226–2237. https://doi.org/10.1021/ma00175a030.

(3) Nölle, J. M.; Jüngst, C.; Zumbusch, A.; Wöll, D. Monitoring of Viscosity Changes during Free Radical Polymerization Using Fluorescence Lifetime Measurements. *Polym. Chem.* **2014**, *5* (8), 2700. https://doi.org/10.1039/c3py01684f.

(4) Wood, L. A. Glass Transition Temperatures of Copolymers. *J. Polym. Sci.* **1958**, *28* (117), 319–330. https://doi.org/10.1002/pol.1958.1202811707.

(5) Vieira, R. A. M.; Sayer, C.; Lima, E. L.; Pinto, J. C. In-Line Andin Situ Monitoring of Semi-Batch Emulsion Copolymerizations Using near-Infrared Spectroscopy. *J. Appl. Polym. Sci.* **2002**, *84* (14), 2670–2682. https://doi.org/10.1002/app.10434.

(6) Alb, A. M.; Enohnyaket, P.; Drenski, M. F.; Head, A.; Reed, A. W.; Reed, W. F. Online Monitoring of Copolymerization Involving Comonomers of Similar Spectral Characteristics. *Macromolecules* **2006**, *39* (17), 5705–5713. https://doi.org/10.1021/ma060800f.

(7) Barnes, S. E.; Sibley, M. G.; Edwards, H. G. M.; Coates, P. D. Process Monitoring of Polymer Melts Using In-Line Spectroscopy. *Transactions of the Institute of Measurement and Control* **2007**, *29* (5), 453–465. https://doi.org/10.1177/0142331207084336.

(8) Ober, C. K.; Lok, K. P.; Hair, M. L. Monodispersed, Micron-Sized Polystyrene Particles by Dispersion Polymerization. *J. Polym. Sci. B Polym. Lett. Ed.* **1985**, *23* (2), 103–108. https://doi.org/10.1002/pol.1985.130230209.

(9) Takahashi, K.; Kato, H.; Saito, T.; Matsuyama, S.; Kinugasa, S. Precise Measurement of the Size of Nanoparticles by Dynamic Light Scattering with Uncertainty Analysis. *Part. Part. Syst. Charact.* **2008**, *25* (1), 31–38. https://doi.org/10.1002/ppsc.200700015.

(10) Qiu, J.; Gaynor, S. G.; Matyjaszewski, K. Emulsion Polymerization of *n* -Butyl Methacrylate by Reverse Atom Transfer Radical Polymerization. *Macromolecules* **1999**, *32* (9), 2872–2875. https://doi.org/10.1021/ma981695f.

(11) Maleki, M. R.; Mouazen, A. M.; Ramon, H.; De Baerdemaeker, J. Multiplicative Scatter Correction during On-Line Measurement with Near Infrared Spectroscopy. *Biosystems Engineering* **2007**, *96* (3), 427–433. https://doi.org/10.1016/j.biosystemseng.2006.11.014.

(12) Rinnan, Å.; Berg, F. van den; Engelsen, S. B. Review of the Most Common Pre-Processing Techniques for near-Infrared Spectra. *TrAC Trends in Analytical Chemistry* **2009**, *28* (10), 1201–1222. https://doi.org/10.1016/j.trac.2009.07.007.

(13) Ito, K.; Kato, T.; Ona, T. Non-Destructive Method for the Quantification of the Average Particle Diameter of Latex as Water-Based Emulsions by near-Infrared Fourier Transform Raman Spectroscopy. *J. Raman Spectrosc.* **2002**, *33* (6), 466–470. https://doi.org/10.1002/jrs.860.

(14) Reis, M. M.; Araújo, P. H. H.; Sayer, C.; Giudici, R. Evidences of Correlation between Polymer Particle Size and Raman Scattering. *Polymer* **2003**, *44* (20), 6123–6128. https://doi.org/10.1016/S0032-3861(03)00669-4.

(15) Houben, C.; Nurumbetov, G.; Haddleton, D.; Lapkin, A. A. Feasibility of the Simultaneous Determination of Monomer Concentrations and Particle Size in Emulsion Polymerization Using in Situ Raman Spectroscopy. *Ind. Eng. Chem. Res.* **2015**, *54* (51), 12867–12876. https://doi.org/10.1021/acs.iecr.5b02759.

(16) Silva, W. K.; Chicoma, D. L.; Giudici, R. In-Situ Real-Time Monitoring of Particle Size, Polymer, and Monomer Contents in Emulsion Polymerization of Methyl Methacrylate by near Infrared Spectroscopy. *Polym Eng Sci* **2011**, *51* (10), 2024–2034. https://doi.org/10.1002/pen.22100.

(17) Gossen, P. D.; Macgregor, J. F.; Pelton, R. H. Composition and Particle Diameter for Styrene/Methyl Methacrylate Copolymer Latex Using UV and NIR Spectroscopy. *Applied Spectroscopy* **1993**, *47* (11), 1852–1870. https://doi.org/10.1366/0003702934066154.

(18) Reis, M. M.; Araújo, P. H. H.; Sayer, C.; Giudici, R. In Situ Near-Infrared Spectroscopy for Simultaneous Monitoring of Multiple Process Variables in Emulsion Copolymerization. *Ind. Eng. Chem. Res.* **2004**, *43* (23), 7243–7250. https://doi.org/10.1021/ie034277u.

(19) Chicoma, D. L.; Sayer, C.; Giudici, R. In-Line Monitoring of Particle Size during Emulsion Polymerization under Different Operational Conditions Using NIR Spectroscopy: In-Line Monitoring of Particle Size during Emulsion Polymerization …. *Macromolecular Reaction Engineering* **2011**, *5* (3–4), 150–162. https://doi.org/10.1002/mren.201000049.

(20) Ambrogi, P. M. N.; Colmán, M. M. E.; Giudici, R. Miniemulsion Polymerization Monitoring Using Off-Line Raman Spectroscopy and In-Line NIR Spectroscopy. *Macromol. React. Eng.* **2017**, *11* (4), 1600013. https://doi.org/10.1002/mren.201600013.

(21) Torraga, M. G. F.; Giudici, R. Stabilizer-Free Dispersion Copolymerization Monitoring by In-Line NIR Spectroscopy. *Ind. Eng. Chem. Res.* **2020**, *59* (35), 15497–15505. https://doi.org/10.1021/acs.iecr.0c02386.

(22) Santos, A. F.; Pinto, J. C. Control and Design of Average Particle Size in Styrene Suspension Polymerizations Using NIRS. *Journal of Applied Polymer Science*. 2000, pp 453–462.

(23) de Faria, J. M.; Machado, F.; Lima, E. L.; Pinto, J. C. In-Line Monitoring of Vinyl Chloride Suspension Polymerization with Near-Infrared Spectroscopy, 1 - Analysis of Morphological Properties. *Macromol. React. Eng.* **2010**, *4* (1), 11–24. https://doi.org/10.1002/mren.200900035.

(24) Fu, Q.; Sun, W. Mie Theory for Light Scattering by a Spherical Particle in an Absorbing Medium. *Appl. Opt.* **2001**, *40* (9), 1354. https://doi.org/10.1364/AO.40.001354.

(25) Cox, A. J.; DeWeerd, A. J.; Linden, J. An Experiment to Measure Mie and Rayleigh Total Scattering Cross Sections. *American Journal of Physics* **2002**, *70* (6), 620–625. https://doi.org/10.1119/1.1466815.

(26) Dzhongova, E.; Harwood, C. R.; Thennadil, S. N. Changes in the Absorption and Scattering Properties in the Near-Infrared Region during the Growth of *Bacillus Subtilis* in Liquid Culture. *Appl Spectrosc* **2009**, *63* (1), 25–32. https://doi.org/10.1366/000370209787169777.

(27) Cubeddu, R.; D'Andrea, C.; Pifferi, A.; Taroni, P.; Torricelli, A.; Valentini, G.; Dover, C.; Johnson, D.; Ruiz-Altisent, M.; Valero, C. Nondestructive Quantification of Chemical and Physical Properties of Fruits by Time-Resolved Reflectance Spectroscopy in the Wavelength Range 650–1000 Nm. *Appl. Opt.* **2001**, *40* (4), 538. https://doi.org/10.1364/AO.40.000538.

(28) Igne, B.; Talwar, S.; Feng, H.; Drennen, J. K.; Anderson, C. A. Near-Infrared Spatially Resolved Spectroscopy for Tablet Quality Determination. *Journal of Pharmaceutical Sciences* **2015**, *104* (12), 4074–4081. https://doi.org/10.1002/jps.24618.

(29) Rey-Bayle, M.; Bendoula, R.; Caillol, N.; Roger, J.-M. Multiangle near Infrared Spectroscopy Associated with Common Components and Specific Weights Analysis for in Line Monitoring. *Journal of Near Infrared Spectroscopy* **2019**, 096703351983006. https://doi.org/10.1177/0967033519830062.

(30) Chen, Y.-C.; Foo, D.; Dehanov, N.; Thennadil, S. N. Spatially and Angularly Resolved Spectroscopy for In-Situ Estimation of Concentration and Particle Size in Colloidal Suspensions. *Anal Bioanal Chem* **2017**, *409* (30), 6975–6988. https://doi.org/10.1007/s00216-017-0672-4.

(31) Gheghiani, M.; Caillol, N.; Henrot, S.; McKenna, T. F. L.; Sheibat-Othman, N. Monitoring of Polymer Content in an Emulsion Polymerization Using Spatially Resolved Spectroscopy in the near Infrared Region and Raman Spectroscopy. *Polym Eng Sci* **2020**, pen.25467. https://doi.org/10.1002/pen.25467.

(32) Savitzky, A.; Golay, M. J. E. Smoothing and Differentiation of Data by Simplified Least Squares Procedures. *Anal. Chem.* **1964**, *36* (8), 1627–1639. https://doi.org/10.1021/ac60214a047.

(33) Geladi, P.; Kowalski, B. R. Partial Least-Squares Regression: A Tutorial. *Analytica Chimica Acta* **1986**, *185*, 1–17. https://doi.org/10.1016/0003-2670(86)80028-9.

(34) Z-Average Particle Size: An Explanation - HORIBA http://www.horiba.com/scientific/products/particle-characterization/education/sz-100/particle-size-by-dynamic-light-scattering-resources/what-is-z-average/ (accessed Aug 16, 2019).

(35) Joudrier, V.; Bourdon, P.; Hache, F.; Flytzanis, C. Characterization of Nonlinear Scattering in Colloidal Suspensions of Silica Particles. *Applied Physics B: Lasers and Optics* **2000**, *70* (1), 105–109. https://doi.org/10.1007/s003400050016.

TOC Graphic

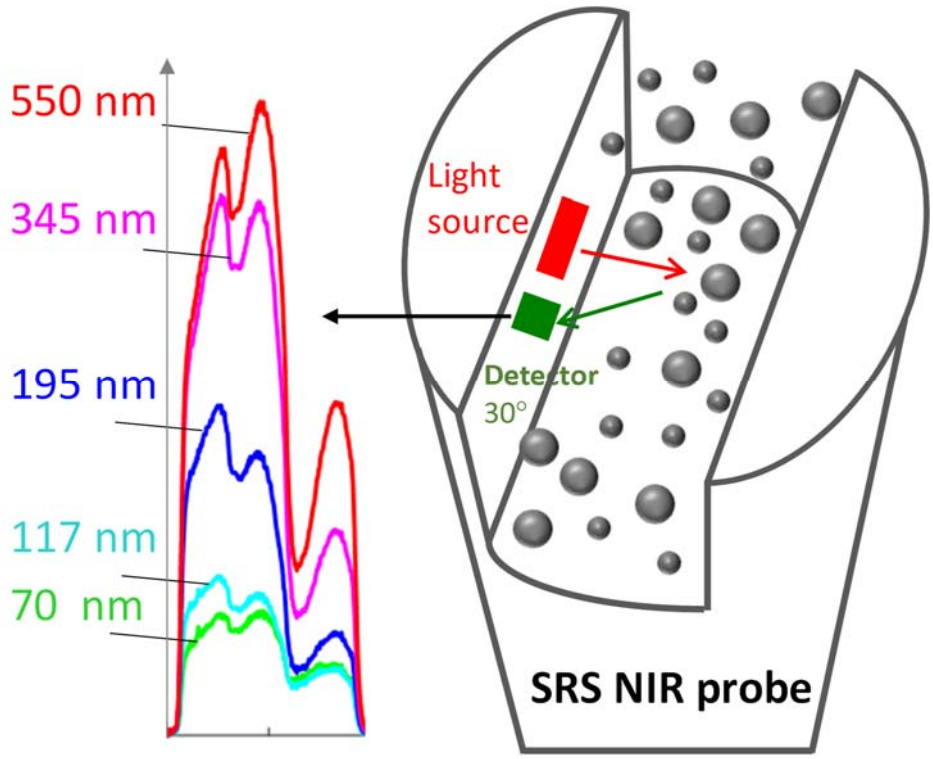
550 nm
345 nm
195 nm
117 nm
70 nm
Light source
Detector
30°
SRS NIR probe